Type IIn supernovae at $z \sim 2$ from archival data

Jeff Cooke[1], Mark Sullivan[2], Elizabeth J. Barton[1], James S. Bullock[1], Ray G. Carlberg[3], Avishay Gal-Yam[4], Erik Tollerud[1]

July 10, 2009

[1] Center for Cosmology, Department of Physics and Astronomy, University of California, Irvine, CA 92697-4574, USA [2] Department of Physics, University of Oxford, Denys Wilkinson Building, Keble Road, Oxford OX1 3RH, UK [3] Department of Astronomy and Astrophysics, University of Toronto, Toronto, ON M5S 3H4, Canada [4] Benoziyo Center for Astrophysics, Weizmann Institute of Science, 76100 Rehovot, Israel

Abstract

Supernovae have been confirmed to redshift $z \sim 1.7$ [1, 2] for type Ia (thermonuclear detonation of a white dwarf) and to $z \sim 0.7$ [1, 3, 4, 5] for type II (collapse of the core of the star). The subclass type IIn [6] supernovae are luminous [7, 8, 9] core-collapse explosions of massive stars [8, 9, 10, 11] and, unlike other types, are very bright in the ultraviolet [12, 13, 14, 15], which should enable them to be found optically at redshifts $z \sim 2$ and higher [16, 14]. In addition, the interaction of the ejecta with circumstellar material creates strong, long-lived emission lines that allow spectroscopic confirmation of many events of this type at $z \sim 2$ for $3-5$ years after explosion [14]. Here we report three spectroscopically confirmed type IIn supernovae, at redshifts $z = 0.808, 2.013$ and 2.357, detected in archival data using a method [14] designed to exploit these properties at $z \sim 2$. Type IIn supernovae directly probe the formation of massive stars at high redshift. The number found to date is consistent with the expectations of a locally measured [17] stellar initial mass function, but not with an evolving initial mass function proposed to explain independent observations at low and high redshift.

The three $z \sim 2$ type IIn supernovae are detected in the Deep component of the Canada-France-Hawaii Telescope Legacy Survey (CFHT-LS) which consists of four fields, each of area one degree-squared, imaged over five years in five ($u^*g'r'i'z'$) filters. Our approach is to monitor $z \sim 2$ galaxies over multiple years and search for flux variations that meet criteria for high-redshift type IIn supernovae. Galaxies are identified using efficient colour-selection techniques [21, 22, 23] tailored to the CFHT-LS and spectroscopically tested using the Vi(r)mos-VLT Deep Survey [24]. The nightly images from a given year (a $5-6$ month "season" of observations) are combined into "seasonal-stacked" images for each filter. The stacked images are sensitive to the slow ($\sim 3-5$ months

at $z \sim 2$) photometric evolution of high-redshift type IIn supernovae as a result of cosmological time dilation, and to events ∼6 times fainter than those detected by the Supernova Legacy Survey that searches the same high-quality data using conventional techniques [25]. Finally, we use the "seasonal-stacked" images for candidate inspection and the nightly exposures to construct high-resolution light curves (see Supplementary Information for more details).

The confirmed $z \sim 2$ type IIn supernovae are the first three supernovae candidates detected in the two fields over four seasons (2003-2006) analysed to date. Candidates must meet conservative criteria that include (1) detection of $\geq 3\sigma$ in the $g'-, r'-$, and $i'-$band "seasonal-stacked" images, (2) flux variation in only one season (the first and last seasons are disregarded for this reason), (3) clean point-source detections in the subtracted images, (4) a priority for events with host galaxy centroid offsets, and (5) $g'r'i'$ light curves that exhibit flux rise times and decay rates consistent with supernova profiles. The criteria are designed to prevent misidentification of active galactic nuclei (AGN; accreting supermassive black holes at the centres of galaxies) and other contaminants that can mimic supernova events to a certain extent.

The $g'r'i'$ light curves for the three $z \sim 2$ supernovae are presented in Fig. 1 and are photometrically consistent with type IIn supernovae behaviour. We confirmed the supernova redshifts (Table 1) from deep spectroscopy obtained using the 10-m telescopes at the W. M. Keck Observatory equipped with the Deep Imaging Multi-Object Spectrograph [26] on 30 September 2008 and 01 October 2008 and with the Low Resolution Imaging Spectrometer [27, 28] on 25 January 2009. The ability to spectroscopically confirm the events as type IIn supernovae via the detection of strong, long-lived emission lines differs dramatically from other SN types that require rapid follow-up to obtain spectral classifications of quickly fading continua.

We detected late-time supernova emission to $> 3\sigma$ significance in the combined 6,000-s exposure of SN 234161 (365 days old, rest-frame; Fig. 2). The features are very similar to those seen at low-redshift, and include ultraviolet shock ionization emission lines (such as semi-forbidden transitions NIV] and NIII] that are extremely rare in AGN), and emission-line strength ratio values (for example, CIV/CIII]) that are not theoretically predicted or observed in AGN. In addition, the combined 5,400-s exposure of SN 19941 (345 days old, rest-frame) exhibits strong blueshifted SiIV and weaker CIV emission attributed to the supernova. We did not detect significant ($> 3\sigma$) supernova emission in the spectrum of SN 219241. This is probably a consequence of the supernova age (855 days old, rest-frame), placing it at an epoch when the emission lines are expected to fade to near or below the spectroscopic threshold of the shorter combined 3,600-s exposure [14]. The detection and eventual decay of type IIn supernova emission lines verify photometric classification, and confirm the ability to study supernova energies and chemistry on an individual basis to high redshift. (See Supplementary Information for spectroscopic and line-emission details.)

Progenitors of type IIn supernovae are believed to be massive stars [10, 11, 8, 9] that sample the high-mass end of the stellar initial mass function

(IMF) of galaxies. Because this method colour-selects a well-controlled population of galaxies over a well-defined volume, a small number of type IIn supernovae can not only give the high-redshift rate of these supernovae, but also provide the first direct probe of the high redshift IMF. For example, an evolving IMF model invoked recently to reconcile indirect high- and low-redshift observations [18, 20, 19] predicts a greater number (by a factor of ~ 3) of $z \sim 2$ type IIn supernovae than a locally measured IMF [17]. Computing the expectations for the volume analysed to date, the confirmed type IIn supernovae presented here are consistent with the relative number predicted using a static local IMF. A relaxation of our conservative supernova criteria and a search for supernovae at greater radii from their host centroids in the complete CFHT-LS dataset will test the validity of this result. Finally, the method presented here provides a means to identify $\sim 40,000$ type IIn supernovae at $z \sim 2$ and to detect events to $z \sim 6$ over the next ten years with 8-m-class deep synoptic optical campaigns, some of which are currently underway and some of which are soon to begin. This cannot be done with any other supernova type or by conventional search practices. As a result, the exceptional properties of type IIn supernovae should enable a seamless study of stellar and galactic processes, ranging from the local Universe to a time shortly after the formation of the first stars.

This work was made possible by the generous support provided by the Gary McCue Postdoctoral Fellowship and the Center for Cosmology at the University of California, Irvine. We acknowledge support from NSERC and the Royal Society. The analysis pipeline used to reduce the DEIMOS data was developed at UC Berkeley with support from NSF grant AST-0071048. The CFHT Legacy Survey relies on observations with MegaCam, a joint project of CFHT and CEA/DAPNIA, at the Canada-France-Hawaii Telescope (CFHT). We used data products from the Canadian Astronomy Data Centre as part of the CFHT Legacy Survey. Some of the data presented here were obtained at the W. M. Keck Observatory. Both observatories are located near the summit of Mauna Kea, Hawai'i. The authors wish to recognize and acknowledge the very significant cultural role and reverence that the summit of Mauna Kea has always had within the indigenous Hawaiian community. We are most fortunate to have the opportunity to conduct observations from this mountain.

The authors declare that they have no competing financial interests.

Correspondence should be addressed to Jeff Cooke (email: cooke@uci.edu).

References

[1] Poznanski, D. *et al.* Supernovae in the Subaru Deep Field: an initial sample and Type Ia rate out to redshift 1.6 *Mon. Not. R. Astron. Soc.* **382**, 1169–1186 (2007).

[2] Riess, A. G. *et al.* The Farthest Known Supernova: Support for an Accelerating Universe and a Glimpse of the Epoch of Deceleration *Astrophysical Journal* **560**, 49–71 (2001).

[3] Botticella, M. T. *et al.* Supernova rates from the Southern inTermediate Redshift ESO Supernova Search (STRESS) *Astronomy & Astrophysics* **479**, 49–68 (2008).

[4] Della Valle, M. *et al.* Hypernova Signatures in the Late Rebrightening of GRB 050525A *Astrophysical Journal* **642**, 103–106 (2006).

[5] Soderberg, A. M. *et al.* An HST Study of the Supernovae Accompanying GRB 040924 and GRB 041006 *Astrophysical Journal* **636**, 391–399 (2006).

[6] Schlegel E. M. A new subclass of Type II supernovae? *Mon. Not. R. Astron. Soc.* **244**, 269–271 (1990).

[7] Richardson, D. *et al.* A Comparative Study of the Absolute Magnitude Distributions of Supernovae *Astronomical Journal* **123**, 745–752 (2002).

[8] Smith, N. *et al.* SN 2006gy: Discovery of the Most Luminous Supernova Ever Recorded, Powered by the Death of an Extremely Massive Star like η Carinae *Astrophysical Journal* **666**, 1116-1128 (2007).

[9] Smith, N. *et al.* SN 2006tf: Precursor Eruptions and the Optically Thick Regime of Extremely Luminous Type IIn Supernovae *Astrophysical Journal* **686**, 467-484 (2008).

[10] Kotak, R. & Vink, J. S. Luminous blue variables as the progenitors of supernovae with quasi-periodic radio modulations *Astronomy & Astrophysics* **460**, 5-8 (2006).

[11] Gal-Yam, A. *et al.* On the Progenitor of SN 2005gl and the nature of Type IIn Supernovae *Astrophysical Journal* **656**, 372-381 (2007).

[12] Fransson, C. *et al.* Optical and Ultraviolet Spectroscopy of SN 1995N: Evidence for Strong Circumstellar Interaction *Astrophysical Journal* **572**, 350–370 (2002).

[13] Fransson, C. *et al.* Hubble Space Telescope and Ground-Based Observations of SN 1993J and SN 1998S: CNO Processing in the Progenitors *Astrophysical Journal* **622**, 991–1007 (2005).

[14] Cooke J. Detecting $z > 2$ Type IIn Supernovae *Astrophysical Journal* **677**, 137–145 (2008).

[15] Brown, P. *et al.* Ultraviolet Light Curves of Supernovae with Swift UVOT *arXiv:0803.1265* , (2008).

[16] Dahlén T. & Fransson, C. Rates and redshift distributions of high-z supernovae *Astronomy & Astrophysics* **350**, 345–367 (1999).

[17] Salpeter, E., E. The Luminosity Function and Stellar Evolution *Astrophysical Journal* **121**, 161-167 (1955).

[18] van Dokkum, P. G. Evidence of Cosmic Evolution of the Stellar Initial Mass Function *Astrophysical Journal* **674**, 29–50 (2008).

[19] Chary, R-R. The Stellar Initial Mass Function at the Epoch of Reionization *Astrophysical Journal* **680**, 32–40 (2008).

[20] Davé, R. The galaxy stellar mass-star formation rate relation: evidence for an evolving initial mass function *Mon. Not. R. Astron. Soc.* **385**, 147–160 (2008).

[21] Steidel, C. C. *et al.* Lyman Break Galaxies at Redshift $z \sim 3$: Survey Description and Full Data Set *Astrophysical Journal* **592**, 728–754 (2003).

[22] Steidel, C. C. *et al.* A Survey of Star-Forming Galaxies in the $1.4 < z < 2.5$ Redshift Desert: Overview *Astrophysical Journal* **604**, 534–550 (2004).

[23] Cooke, J. *et al.* Survey for Galaxies Associated With $z \sim 3$ Damped Ly-α Systems. I. Spectroscopic Calibration of u'BVRI Photometric Selection *Astrophysical Journal* **621**, 596–614 (2005).

[24] Le Fèvre, O. *et al.* Virmos-VLT deep survey (VVDS) *SPIE* **4834**, 173–182 (2003).

[25] Neill, J. D. *et al.* The Type Ia Supernova Rate at z 0.5 from the Supernova Legacy Survey *Astronomical Journal* **132**, 1126–1145 (2006).

[26] Faber, S. M. *et al.* The DEIMOS spectrograph for the Keck II Telescope: integration and testing *SPIE* **4841**, 1657–1669 (2003).

[27] Oke, J. B. *et al.* The Keck Low-Resolution Imaging Spectrometer *Pub. of the Astron. Soc. of the Pacific* **107**, 375–385 (1995).

[28] McCarthy, J. K. *et al.* Blue channel of the Keck low-resolution imaging spectrometer *SPIE* **3355**, 81–91 (1998).

[29] Riess, A. G. *et al.* Identification of Type Ia Supernovae at Redshift 1.3 and Beyond With the Advanced Camera for Surveys on the Hubble Space Telescope *Astrophysical Journal Letters* **600**, 163–166 (2004).

[30] Shapley, A. E. *et al.* Rest-frame Ultraviolet Spectra of $z \sim 3$ Lyman Break Galaxies *Astrophysical Journal* **558**, 65–89 (2003).

SN	R.A. (J2000)	Dec. (J2000)	Host m_r	Date of Outburst	SN m_r	SN M_{UV}	Separation kpc	Redshift z
19941	02 24 11.147	-04 57 58.41	25.16 ± 0.07	24Nov2005	$25.6^{+0.2}_{-0.3}$	$-19.5^{+0.2}_{-0.3}$	1.1 ± 0.8	2.357 ± 0.002
234161	02 24 33.271	-04 26 31.04	24.93 ± 0.07	27Sep2005	$25.2^{+0.2}_{-0.2}$	$-19.6^{+0.2}_{-0.2}$	2.8 ± 0.8	2.013 ± 0.002
219241	22 14 47.351	-17 46 11.62	24.12 ± 0.04	08Jul2004	$24.7^{+0.1}_{-0.1}$	$-18.2^{+0.1}_{-0.1}$	2.0 ± 0.7	0.808 ± 0.001

Table 1: High-redshift supernova and host galaxy properties. Both the dates of outburst and the supernova (SN) magnitudes are determined from the light curves. Supernova apparent r'-band magnitudes (mr') are at peak brightness and corresponding absolute ultraviolet magnitudes (M_{UV}) are estimated at the r'-band effective rest-frame wavelengths. Separations are measured between the centroids of the supernovae and their host galaxies and are accurate to ± 0.52 pixels, which corresponds to a physical separation of $0.7 - 0.8$ kpc (see Supplementary Information).

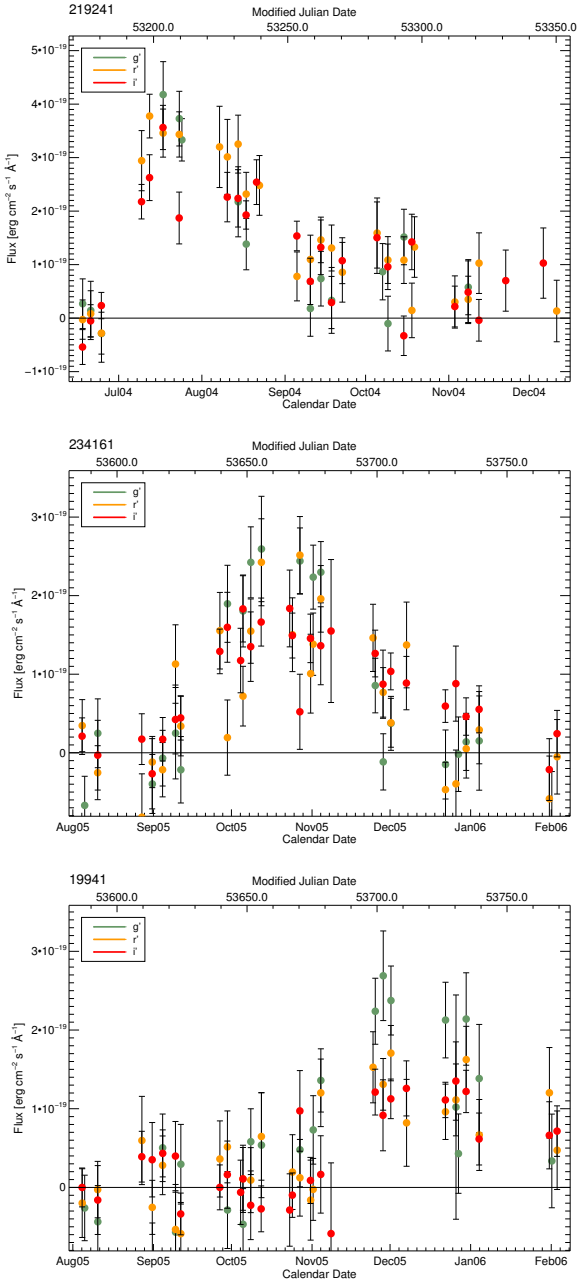

Figure 1: Multi-colour light curves of the three high-redshift supernovae. Top to bottom: SN 219241 ($z = 0.808$), SN 234161 ($z = 2.013$), and SN 19941 ($z = 2.357$). The flux and 1σ uncertainties for the $g'r'i'$ optical filters shown here probe the rest-frame ultraviolet flux for these events. The seasonal integrated flux from each supernova is detected at $3-8.4\sigma$ over the host galaxy flux in each filter. Because type Ia supernovae exhibit very little flux shortward of ~ 300 nm as a result of efficient FeII scattering of ultraviolet photons [29], this classification is ruled out. We find that the ultraviolet luminosity and evolution of the supernovae in each filter are most consistent with type IIn events (see Supplementary Information).

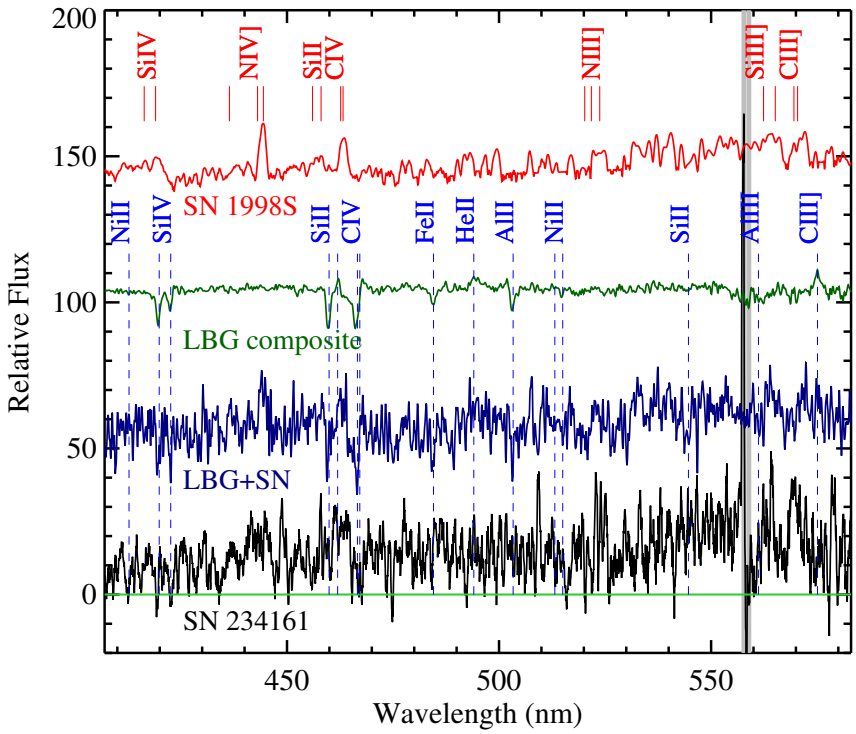

Figure 2: Four spectra with vertical offsets to help illustrate the detection of line-emission from SN 234161. **(a)** The ultraviolet spectrum (red) of the low-redshift SN 1998S [13] (day 485) shifted and flux corrected to $z = 2.013 - 2,500$ km s^{-1} ($-2,500$ km s^{-1} corresponds to $\Delta z = -0.026$; best fit match to SN 234161 emission). The short solid vertical lines indicate the positions of expected type IIn supernovae emission-line features. **(b)** A composite $z \sim 3$ galaxy spectrum [30] (green) representative of typical $z \sim 2-3$ galaxies using our colour selection. Dashed vertical lines indicate the expected positions of interstellar ultraviolet features. **(c)** Convolution of the composite galaxy and SN 1998S spectra (blue) with Gaussian noise added consistent with that of the data. **(d)** The data for SN 234161 (day 365; black). The thick grey vertical line marks the position of a bright night sky emission line that is difficult to subtract cleanly from the faint spectrum. The effect of the supernova emission on the convolved spectrum includes the SiIV 139.4, 140.3 nm profile, excess flux from NIV] 146.1, 148.3, 148.8 and NIII] 174.1, 174.7, 175.3 nm near 440 and 520 nm, respectively, excess flux and profile of CIV 154.8, 155.0 nm near 460 nm, and the rise in the continuum beyond ~ 530 nm. Comparison of the data to the convolved spectrum shows that SN 234161 is consistent with an average $z \sim 2 - 3$ galaxy experiencing a SN 1998S-like event with emission-line peaks blueshifted 2500 km sec^{-1} (low-redshift type IIn supernovae also exhibit blue-shifted emission peaks). In addition, SN 234161 exhibits strong CIII] 190.7, 190.9 nm supernova emission near 570 nm. We remark that SN 1998S and type IIn SN 1995N [12] exhibited CIII] emission of similar relative strength to SN 234161 at earlier (day 238) and later (day 943) times, respectively.

Supplementary information

Here we describe in more detail the image stacking process (§1), the galaxy colour-selection technique (§2), and the supernova (SN) UV magnitudes and decay rates derived from the images and light curves (§3 & 4). In addition, we present the spectroscopic observations for the three $z \sim 2$ SNe (§5) and discuss evidence for SN line emission detection from SN 234161 and SN 19941 (§6).

1 Image stacks

"Seasonal-stacked" images in the two fields are made from data from the individual nights observed in each of the g', r', and i' filters. A precise astrometric solution, accounting for geometrical distortion, is assigned to every image frame, and the images resampled to a common pixel coordinate system. The seeing (the FWHM of the point-spread function) and photometric quality are determined by flux measurements of tertiary standard stars in the CFHT-LS fields compiled by the SNLS team. These tertiary standards provide photometric zeropoints to the Vega system and are derived from observations of secondary standard stars [31]. Two-dimensional sky variation is removed from each frame by fitting the background spatially and subtracting the resultant fit. Each individual frame has a weight-map associated with it, containing the uncertainty in each pixel from considerations of photon noise from the sky background and object photons. Known bad pixels and saturated pixels are assigned a weight of zero. The stacks are then made from the highest-quality data taken in each year as part of CFHT-LS: all individual images entering the stacks have seeing $< 0.75''$ FWHM. The resampled frames that pass this cut are combined using a weighted average, with a 3σ clipping to remove artifacts such as satellite trails and cosmic-rays. Typical exposure times for the final stacked images range from 10,000 seconds (in g') to 50,000 seconds (in i').

2 Galaxy colour-selection

We combine the "seasonal-stacked" images from all four years into "super-stacked" images to colour-select high-redshift galaxies. In this manner we reach deeper than the "seasonal-stacked" images alone and are able determine galaxy colours with photometric uncertainties ≤ 0.2 mag for galaxies to $m_{r'} \sim 27$. We detect sources in the field using *SExtractor* [32] software and use the segmentation map generated from the "super-stacked" images to monitor the flux of selected galaxies year-to-year in the "seasonal-stacked" images. The higher sensitivity of the "super-stacked" images enable a more complete pixel definition of the luminous extent of each galaxy for optimal reference segmentation maps. In addition, the combination of four seasons effectively dilutes any potential colour contribution to the host galaxy as a result of part or all of a SN event that may affect the colour selection. We note that $z \sim 2$ SNe IIn are detectable in the

CFHT-LS data for $\sim 3-5$ months, observed-frame. Any significant contribution from a detectable SN would result in a net flat or bluer addition the host galaxy colour in a given "seasonal-stacked" image and our colour criteria include the bluest galaxies. A somewhat redder SN contribution in the UV would come from the fraction of an event caught after peak brightness which would in turn be quite faint in integrated light in the particular "seasonal-stacked" image and thereby contribute very little to the four-season "super-stacked" image.

We filter $z \geq 1$ galaxies from the detected sources using a colour-selection technique specifically designed for the CFHT MegaCam. We determine the colours of 10 different galaxy templates evolved from $z = 0$ to high redshift by convolving the templates with (1) the throughput of the CFHT MegaCam $u^*g'r'i'z'$ filters, (2) the MegaCam CCD quantum efficiency, (3) the atmospheric extinction of Mauna Kea, and (4) an adopted high-redshift prescription [33] for the expected decrement of flux shortward of Ly-α and the Lyman limit as a result of intervening systems and intrinsic absorption. We use the spectroscopic catalogue of the Vi(r)mos-VLT Deep Survey (VVDS) [24] to test our CFHT-LS colour selection criteria and find that 83% of the galaxies common to both surveys that have both VVDS high-confidence redshift qualifiers and that meet our colour criteria have redshifts $z > 1$. The colour cuts that isolate $z \sim 2$ and $z \sim 3$ galaxies result in redshift distributions $\langle z \rangle = 1.68 \pm 0.34$ and $\langle z \rangle = 3.17 \pm 0.41$, respectively (there are too few galaxies for a meaningful distribution for our $z > 3$ colour cuts). We monitor all sources that meet these color criteria and consider a relaxed color cut that includes $z > 1$ sources.

3 Supernova photometric detection

SNe IIn have a magnitude distribution $\langle M_B \rangle = -19.0 \pm 0.3$, $\sigma = 0.92$ [7] and UV luminosities ~ 1.0 magnitude fainter near peak brightness [13,][34, 35]. SNe template analyses show that $\sim 93\%$ of all SN detections at $z \geq 2$ are expected to be SNe IIn [16,14] as a result of their strong intrinsic UV luminosity. We searched the CFHT-LS data for events are that meet the criteria discussed in the main Letter that includes a 3σ flux variation over the host galaxy flux in each of the $g'r'i'$ filters. Of the initial four $z \sim 2$ SN candidates, two SN events (SN 234161 and SN 19941) meet the $\langle z \rangle = 1.68 \pm 0.34$ and $\langle z \rangle = 3.17 \pm 0.41$ colour-selection and the remaining two events (SN 219241 and SN 352912) meet relaxed colour cuts that select galaxies with redshifts above $z \sim 1$. Follow-up spectroscopy (§5) of SN 234161 and SN 19941 confirmed host redshifts of $z = 2.0125$ and $z = 2.3565$. In addition, we have obtained spectroscopy of SN 219241 and find the host redshift to be $z = 0.8078$. From the above results and the efficiency of our colour selection, we expect the SN 352912 to have a high likelihood to be a $z \geq 1$ event.

The SNe discussed in the main Letter are detected at the following significance above their host galaxy flux in the g', r', and i' seasonal-stacked images, respectively, SN 219241: $6.4, 6.7, 8.4$; SN 234161: $3.0, 3.9, 4.2$; and SN 19941: $3.1, 5.1, 4.9$. These are determined using the SN integrated magnitudes in the

seasonal-stacked images and are $0.6 - 1.2$ magnitudes fainter in a given filter as compared to the peak magnitudes determined from the light curves. Figure 3 displays the r'-band images of the three SNe. Each SN host galaxy is shown as it appeared in the 2004 and 2005 season and is indicated by a circle centred on its flux centroid. The SNe directly affect the appearance of the host galaxy in each case. The subtracted images for both seasons are also shown. The seasons that do not include the SNe help to illustrate the clean subtraction possible with the high-quality CFHT-LS images. The SNe are immediately obvious in the seasons with detections and have measurable offsets from their host galaxy centroids. The subtracted images are similar in the g' and i'-bands, as suggested by the detection significance above, and the SN offsets from their host galaxy flux centroids are consistent for each event filter to filter.

The seeing in the "seasonal-stacked" images is found to be $\sim 0.7''$ FWHM and stable across the images and over the four epochs. We subtracted the average flux of the "seasonal-stacked" images from the combined three adjacent years to construct the subtracted images. The three SNe exhibit clean radial profiles with FWHMs equivalent to that of nearby point sources in the field. The pixel scale of the CFHT MegaCam is $0.187''$ pixel^{-1} and corresponds to $1.4-1.6$ kpc, physical, over $0.8 < z < 2.4$. As listed in Table 1 of the main Letter, the SNe have $1.1 - 2.8$ kpc separations from their host galaxy centroids. We tested the accuracy of these separations by measuring the centroids of a galaxy sample that includes the SN host galaxies and galaxies with similar magnitude. We determined that the centroid measurements are accurate to ± 0.360 pixels, 1σ, in images tested season-to-season and ± 0.175 pixels, 1σ, when tested filter-to-filter for a given season. The SN centroids in the subtracted images were tested in an identical manner and found to be accurate to ± 0.493 pixels, 1σ, filter-to-filter in their respective outburst season. We conclude that the SN-host centroid separations are accurate to ± 0.523 pixels, 1σ. This corresponds to $0.098''$ using the CFHT-LS plate scale and $0.74 - 0.82$ kpc for the range of SN redshifts presented here.

We performed an additional test of the separations between the centroids of known AGN and their host galaxies. These are AGN found to exhibit a flux variation during the seasons probed by the CFHT-LS data and have host galaxies $\sim 1 - 2$ magnitudes brighter than the host galaxies tested above. We find the separations accurate to ± 0.152 pixels, 1σ. Although we expect the centroid uncertainties to behave as a function of magnitude, this test provides a sense of the separation uncertainty for known AGN in host galaxies with relatively similar magnitudes and demonstrates the quality of the CFHT-LS imaging dataset. As a result, the measured SN separations from their host galaxy centroids are real, however SN 19941 is only significant to $\sim 1\sigma$.

4 Light curves

The flux evolution for each of the three $z \sim 2$ SNe is presented in Figure 1 of the main Letter and the magnitude information for the $g'r'i$ filters is listed in

Table 2 below. The uncertainties in the absolute magnitudes are dominated by the photometry with a negligible contribution from the uncertainties in redshift. The strong detection and evolution of flux in the $g'r'i'$ filters, that probe the rest-frame UV for these SNe, places immediate constraints on their classification. First, type Ia SNe show very little flux shortward of $\sim$ 300 nm from efficient scattering of UV photons [29] and would be below the sensitivity of the seasonal-stacked images at $z \geq 0.7$. This rules out a type Ia SNe for these events. Second, type Ib/c and type II SNe, other than SNe IIn, have luminosities too low, and/or that rise and decline too rapidly and remain essentially flat [15] in the UV as compared to that observed for SN 219241, SN 234161 and SN 19941. Instead, the peak UV magnitudes and evolution of are consistent with those of SNe IIn. We tested the intrinsic UV luminosity of all SN types and find that $> 90\%$ of all $z \geq 0.8$ detections in the CFHT-LS g'-band data are expected to be SNe IIn.

Table 3 lists the flux decay rates for each SN. The rest-frame bandpasses that correspond to the observed g', r', and i'-band filters for each SN are arbitrarily indicated as UV1, UV2, and UV3, respectively. SNe IIn have varying decay rates in the optical, but are essentially cooling blackbodies in the UV at early times. We use the expectations of a low extinction, cooling blackbody guided by the UV continuum evolution of SN 1998S [13] to generate a model for the SNe IIn UV decay rates. We compute the rest-frame bandpass of the observations for each SN and the expected decay rate considering the appropriate time dilation. The relevant values of the model are also listed in Table 3. The SNe closely follow the UV decay rate expectations of the model events at the determined redshifts. Moreover, these values are in close agreement to the publicly available *Swift* UVOT data of SN 2007pk and SN 2008am *(http://heasarc.nasa.gov/docs/swift/sne/swift_sn.html)*.

5 Spectroscopy

We obtained low-resolution spectroscopy of SN 219241 and SN 234161 at the W. M. Keck Observatory (Keck) on 30 September 2008 and 01 October 2008. We used the DEep Imaging Multi-Object Spectrograph (DEIMOS) [26] with the 600 line mm^{-1} grating and a multi-object spectroscopic wavelength coverage of $400 - 900$ nm. We acquired three 1200s exposures of SN 219241 and five 1200s exposures of SN 234161. The data were reduced using the UCB *spec2d* pipeline[1]. Because DEIMOS is not sensitive below $\sim$ 400 nm and because bright night sky emission lines begin to dominate the spectra longward of $\sim$ 800 nm, the data were most effective in securing $z \leq 1$ redshifts of the faint host galaxies from strong rest-frame optical features such as [OII]λ 372.7 nm and Balmer features and $z \geq 2.3$ redshifts from strong rest-frame UV features that include prominent Ly-α and ISM absorption features. Objects with redshifts between $1 < z < 2$ fall in the "redshift desert" which is a range of redshift where galaxies exhibit flat continua and no strong identifying features in observed-frame optical

[1] http://astro.berkeley.edu/ cooper/deep/spec2d/

wavelengths. Nevertheless, the UV absorption features over these rest-frame wavelengths have been well-studied and the characteristic flat continua help to make $z \sim 2$ galaxy colour-selection very efficient [22,][36]. In addition to the DEIMOS data, we obtained low-resolution spectroscopy of SN 19941 on 25 January 2009 using the Low-Resolution Imaging Spectrometer (LRIS) [27,28] at Keck. We used the 400 line mm^{-1} grism blazed at 340 nm and the 400 line mm^{-1} grating blazed at 850 nm to utilise both the blue and red arms of LRIS. The excellent blue sensitivity of LRIS resulted in $\sim 320 - 900$ nm wavelength coverage. The data were reduced using conventional methods that include IRAF and IDL tasks and analysed with in-house code.

Figure 4 presents the DEIMOS and LRIS spectra for the three high-redshift SNe. The $z = 0.8078$ host galaxy of SN 219241 exhibits strong [OII]λ 372.7 emission and Ca H&K absorption lines. SN 234161 host galaxy has a best fit redshift of $z = 2.0125$ from a cross-correlation of 23 ISM absorption features that include SiIV λ 139.4, 140.3, CIV λ 154.8, 155.1, MgI λ 202.6, 285.2, and FeII λ234.4, 237.5, 238.3 after omitting those near bright night sky emission lines. SN 19941 exhibits strong Ly-α emission and is found to have a redshift of $z = 2.3565$ from a best fit to multiple ISM absorption features. Both SN 19941 and SN 234161 use a prescription [37] to estimate the systemic redshift of the host galaxy from the observed blueshifted ISM features and redshifted Ly-α emission as a result of galactic winds. The spectrum of SN 19941 shows a relatively broad emission line near rest-frame ~ 137 nm (~ 460 nm observed-frame) and is discussed below.

6 Detection of type IIn supernova emission

In §3 and §4, we showed that the rest-frame UV photometry and light-curve evolution of the three SNe best fit that of SNe IIn. To confirm this, we search the spectroscopy for evidence of the strong, long-lived emission lines that define the IIn classification. The emission lines are expected to remain above the spectroscopic thresholds of 8m-class telescopes using $\sim$ 4-hour exposures for $\sim 2 \cdot (1+z)$ years after outburst [14]. In addition, the emission lines peaks of SNe IIn can have a $\sim 1000 - 4000$ km s^{-1} blueshift [13][38, 39] relative to the host galaxy velocity and evolve with time.

6.1 SN 219241 —

This event was 855 days old, rest-frame, at the time observation. At this late stage, SNe IIn emission lines are expected to be near, or below, the threshold of detection with a $\sim$ 4-hour observation. Although the observing conditions were excellent ($0.4''$ seeing FWHM), our combined 3600s exposure was likely insufficient for significant emission-line detection. As a result, we do not have confident detection of SN line emission from SN 219241. Deeper optical or IR observations in the very near future may provide the sensitivity to detect SN emission or to rule out a IIn classification. As a result, the IIn classification is

based on the UV photometry.

6.2 SN 234161 —

We searched for SN IIn emission line evidence in the combined 6000s exposure obtained under same excellent seeing conditions as SN 219241. This SN was observed 365 days old, rest-frame, and caught at a time when SNe IIn emission lines are expected to be near maximum and above the detection threshold. We detect NIV] $\lambda\lambda$ 146.1, 148.3, 148.8, CIV $\lambda\lambda$ 154.8, 155.0, CIII] $\lambda\lambda$ 190.7, 190.9, and potentially NIII] $\lambda\lambda$ 174.1, 174.7, 175.3 nm emission to $> 3 - 18\sigma$ significance (NIII] emission-line measurements are less reliable because they fall near a subtracted weak night sky emission line). These emission lines arise from circumstellar interaction and are found in low-redshift SNe IIn spectra [12,13].

Figure 5 is similar to Figure 2 in the main Letter but presents the spectrum of SN 234161 separated in bluer and redder wavelength regions for more detailed inspection. Because the signal-to-noise ratio (SNR) of the spectrum is only a few (host galaxy $m_{r'} = 24.9$) and the emission lines from the SN at such a high redshift are faint, we present a high-redshift galaxy composite spectrum and the spectrum of SN 1998S as an aid. Figure 5 steps through the spectra by presenting from top to bottom: (a) the spectrum of SN 1998S [13] at day 485 shifted and flux corrected to $z = 2.0125$ and blueshifted by 2500 km s^{-1} to match the best-fit to the SN emission observed in SN 234161, (b) a composite spectrum of 800 $z \sim 3$ Lyman break galaxies (LBGs) [30] corrected to $z = 2.0125$ that is representative of $z \sim 2 - 3$ galaxies [21,22] color-selected via the technique presented here, (c) a convolution of the composite LBG and SN 1998S spectra with Gaussian noise added to match that of the data, followed by (d) the spectrum of SN 234161. Comparison of the feature profiles and overall continuum shape of the data to the convolved spectrum show the data is consistent with our interpretation of a $z = 2.0125$ galaxy hosting a SNe IIn event with -2500 km s^{-1} offset emission. We use the spectrum of the type IIn(/L) SN 1998S here because it is the only high-quality multiply-sampled UV SNe IIn spectrum to date. We use the older (day 943) single observation of the UV spectrum of SN 1995N [12] throughout our analysis as well which exhibits similar emission lines and relative line-strengths and ratios as those seen in SN 234161.

Some of the effects of the SN can be seen in (1) the continuum profile near 420 nm and the change in the SiIV doublet line strength appearance in both the convolved spectrum and the data as a result of SN SiIV emission, (2) the excess emission on a flat featureless section of the galaxy spectrum near 440 nm attributed to SN NIV] multiplet emission, (3) the continuum profile and excess flux near 460 nm attributed to SN CIV emission and host galaxy SiII and the CIV absorption features, (4) excess flux near 525 nm attributed to SN NIII] emission, and (5) the clean detection of CIII] and weaker SiIII] emission from the SN near 570 nm in the data. The spectrum of SN 1998S shown here is 120 days older than SN 234161. SN 1998S exhibited stronger NIII] and CIII] emission at earlier times [13] as did SN 1995N at a later time [12].

6.3 SN 19941 —

This SN was 345 days old, rest-frame, at the time of the LRIS observations. The salient feature in the host galaxy spectrum is the strong Ly-α emission near observed wavelength 410 nm. Cross-correlation with ISM absorption features results in a best fit redshift of $z = 2.3565$. This is the highest redshift SN ever detected. SN 19941 exhibited a flux increase in only one season and was stable in three, mimicking expected SN behavior, and shows no evidence of AGN emission lines. As with SN 234161 above, this SN is in the time regime when the emission lines from the circumstellar interaction are expected to be near their strongest. This spectrum shows a strong, relatively broad emission line near ~ 460 nm (~ 137 nm rest-frame) that may be the result of blueshifted SiIV $\lambda\lambda$139.4, 140.3 nm emission from the SN. We also find excess CIV and HeII 164.0 nm flux near observed 515 and 550 nm, respectively, which would be in accordance with this interpretation. The SNR of the reduced spectrum obtained with the less sensitive red CCD of LRIS was too low to make any significant assessment other than the lack of strong emission redward of ~ 560 nm (~ 170 nm, rest-frame). This event will require further analysis and deep, high-SNR spectroscopy to search for line evolution.

Over the UV wavelength range probed in this work, the main features that distinguish the SN detections from AGN are the NIV], NIII] and CIII] strengths and their ratios with CIV. SN 234161 exhibits $\sim 1:1$ CIV/NIV] ratio and stronger CIII] than CIV, with CIV/CIII] ~ 0.3. These strengths are similar to that seen in the two available late-time SNe IIn UV spectra; namely that of SN 1995N and SN 1998S [12,13]. Over similar epochs, SN 1995N and SN 1998S exhibit CIV/NIV] ratios of $\sim 0.6-3$ and CIV/CIII] ratios of $0.3-1$. In contrast, the SDSS QSO composite spectrum [40] shows no evidence of NIV] emission and has a CIV/NIII] ratio of ~ 66.

Both NIV] and NIII] are indicators of shock ionisation and only about a dozen known objects at high redshift (including AGN, radio galaxies, QSOs, and normal galaxies) exhibit these lines in emission at a significant level. Rare AGN that do show these features, average a CIV/NIV] ratio of $\sim 20-25$, compared to ~ 1 for SN 234161. These rare AGN still maintain CIV/CIII] ratios of $1.5-2.0$ as is the case for normal AGN (cf., CIV/CIII] ~ 0.3 for SN 234161). Of all objects at high redshift, including normal galaxies, we are aware of only one object in the literature, DLS 1053+0528 [41] that shows equivalent or stronger NIV] emission as compared to CIV. This object does not show other emission lines indicative of shock ionisation as those seen in SNe IIn (e.g., NIII]). CIII] information is not presented for this object. In summary, the UV emission lines seen in the host galaxy spectra of SN 234161 and SN 19941 are unlike AGN and are seen with the expected strengths, line ratios, and blueshifted emission peaks reminiscent of SNe IIn.

References

[31] Landolt, A. UBVRI photometric standard in the magnitude range 11.5-16.0 around the celestial equator *Astronomical Journal* **104**, 340–491 (1992).

[32] Bertin, E. & Arnouts, S. SExtractor: Software for source extraction *Astron. & Astroph. Supp. Series* **117**, 393–404 (1996).

[33] Madau, P. Radiative transfer in a clumpy universe: The colors of high-redshift galaxies *Astrophysical Journal* **441**, 18–27 (1995).

[34] Immler, S. & Pooley, D. Swift Observations of SN 2006bv in UGC 7848 *The Astronomer's Telegram* **802**, 1–1 (2006).

[35] Immler, S. & Brown, P. J. Swift Observations of SN 2007bb *The Astronomer's Telegram* **1053**, 1–1 (2007).

[36] Adelberger, K. L. *et al.* Optical Selection of Star-forming Galaxies at Redshifts $1 < z < 3$ *Astrophysical Journal* **607**, 226–240 (2004).

[37] Adelberger, K. L. *et al.* Galaxies and Intergalactic Matter at Redshift $z \sim 3$: Overview *Astrophysical Journal* **584**, 45–75 (2003).

[38] Filippenko, A. V. The 'Seyfert 1' optical spectra of the type II supernovae 1987F and 1988I *Astronomical Journal* **97**, 726–734 (1989).

[39] Leonard, D. L. *et al.* Evidence for Asphericity in the Type IIN Supernova SN 1998S *Astrophysical Journal* **536**, 239–254 (2000).

[40] Vanden Berk, D. E. *et al.* Composite Quasar Spectra from the Sloan Digital Sky Survey *Astronomical Journal* **122**, 549–564 (2001).

[41] Glikman, E. *et al.* Discovery of Two Spectroscopically Peculiar, Low-Luminosity Quasars at $z \sim 4$ *Astrophysical Journal Letters* **663**, 73–76 (2007).

SN	Redshift z	$m_{g'}$ peak	$m_{r'}$ peak	$m_{i'}$ peak	M_{UV1} peak	M_{UV2} peak	M_{UV3} peak
219241	0.8078 ± 0.0010	$25.14^{+0.15}_{-0.17}$	$24.73^{+0.11}_{-0.12}$	$24.35^{+0.12}_{-0.13}$	$-17.75^{+0.15}_{-0.17}$	$-18.16^{+0.11}_{-0.12}$	$-18.54^{+0.12}_{-0.13}$
234161	2.0125 ± 0.0021	$25.65^{+0.25}_{-0.32}$	$25.17^{+0.19}_{-0.24}$	$25.07^{+0.26}_{-0.34}$	$-19.12^{+0.25}_{-0.32}$	$-19.61^{+0.19}_{-0.24}$	$-19.71^{+0.26}_{-0.34}$
19941	2.3565 ± 0.0022	$25.61^{+0.21}_{-0.26}$	$25.59^{+0.20}_{-0.25}$	$25.40^{+0.34}_{-0.49}$	$-19.46^{+0.21}_{-0.26}$	$-19.49^{+0.20}_{-0.25}$	$-19.68^{+0.34}_{-0.49}$

Table 2: Redshift and magnitude information for the three high-redshift SNe. Magnitudes are at or near maximum brightness as determined from the light curves. Absolute UV magnitudes are estimated for the effective rest-frame wavelengths probed by the $g'r'i'$ filters. UV1, UV2, and UV3 correspond to the g', r' and i'-bands, respectively.

SN	UV1 (g') nm	UV1 Decay mag day^{-1}	UV2 (r') nm	UV2 Decay mag day^{-1}	UV3 (i') nm	UV3 Decay mag day^{-1}
219241 ($z = 0.8078$)	265	0.079	350	0.045	420	0.044
IIn model	270	0.096	370	0.052	420	0.042
234161 ($z = 2.0125$)	160	0.175	210	0.102	250	0.064
IIn model	170	0.159	220	0.105	270	0.098
19941 ($z = 2.3565$)	145	0.205	190	0.129	225	0.119
IIn model	125	0.204	170	0.152	220	0.112

Table 3: Supernova decay rates. Listed are the effective UV wavelengths probed by the g, r', and i'-band filters and estimated decay rates taken from the supernova light curves over $\sim 15 - 35$ days, rest-frame, following peak or near peak brightness. Below each observed value is the expected value from the model. Similar to Figure 2, UV1, UV2, and UV3 correspond to the rest-frame wavelengths probed by the g', r' and i'-bands, respectively. See text for details.

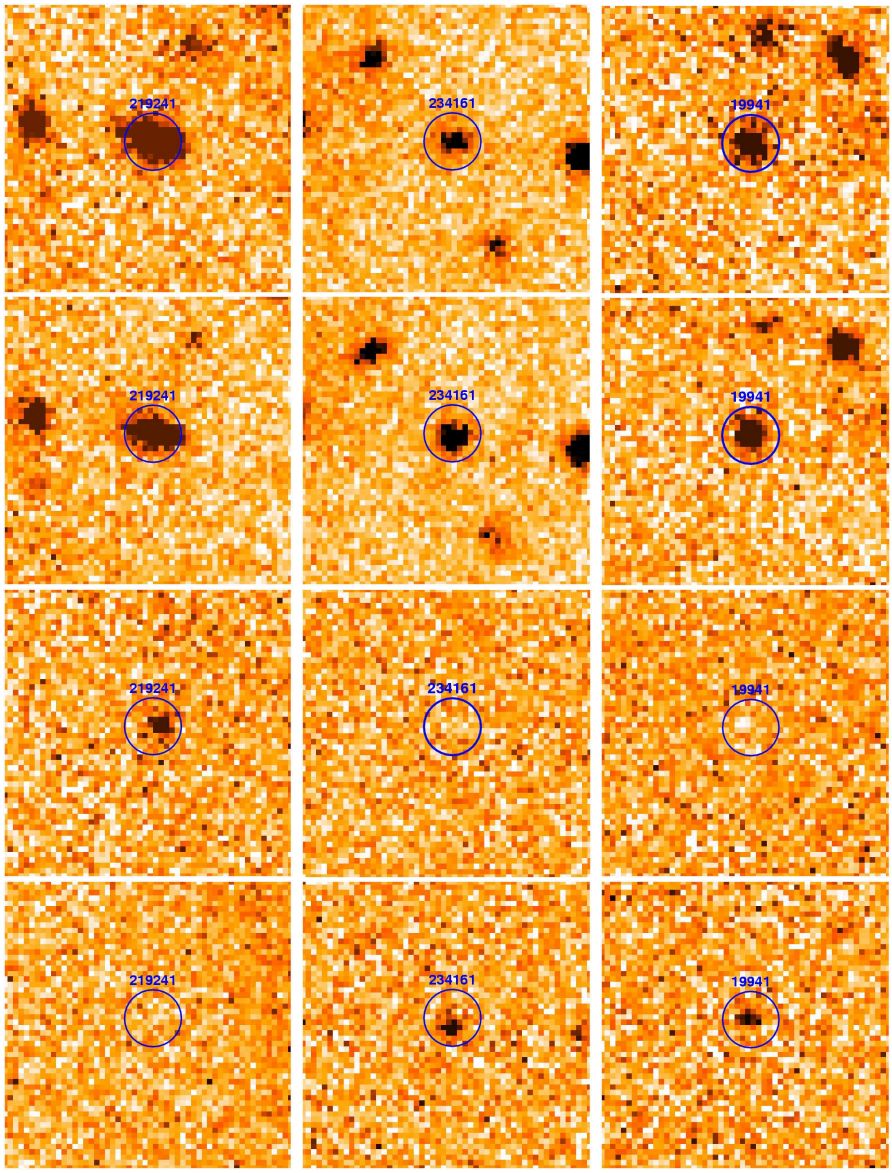

Figure 3: Images and subtracted images in the r'-band for the three supernovae and their host galaxies. Four $10'' \times 10''$ image sections are shown vertically for each supernova and are centred on their respective host galaxy. Rows from top to bottom: Season 2004, season 2005, the subtracted image in 2004, and the subtracted image in 2005. Columns from left to right, the images are of SN 219241, SN 234161, and SN 19941. Each supernova exhibits a clean point-source detection in the subtracted image for each filter and a $\sim 1 - 3$ kpc, physical, offset from its host galaxy centroid.

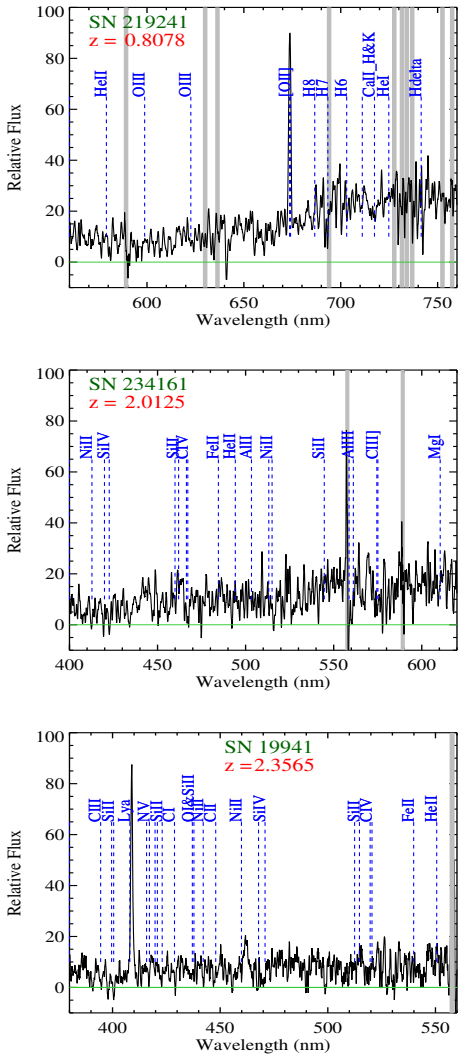

Figure 4: Spectra of the high-redshift supernovae and host galaxies. Thick vertical lines denote the positions of bright night sky emission lines that can be difficult to subtract cleanly from faint spectra. The horizontal green line represents zero flux and the vertical dashed lines indicate expected transitions and are labelled. *Top:* Strong [OII]λ 372.7 emission, CaII$\lambda\lambda$ 393.4, 396.8 absorption, and the break in the continuum near 400 nm are the dominant features that identify the $z = 0.8078$ spectrum of SN 219241. *Centre:* The redshift of SN 234161 was determined by cross-correlation of 23 of 30 UV transitions that did not fall near bright night sky emission lines. We find a best fit redshift of $z = 2.0125$ when considering the effect of the supernova emission lines (see Figure 5). *Bottom:* The SN 19941 host galaxy exhibits strong identifying Ly-α emission. The relatively strong blueshifted SiIV $\lambda\lambda$ 139.4, 140.3 nm and weaker CIV $\lambda\lambda$ 154.8, 155.0 nm and HeII 164.0 nm emission are tentatively assumed to originate from the supernova

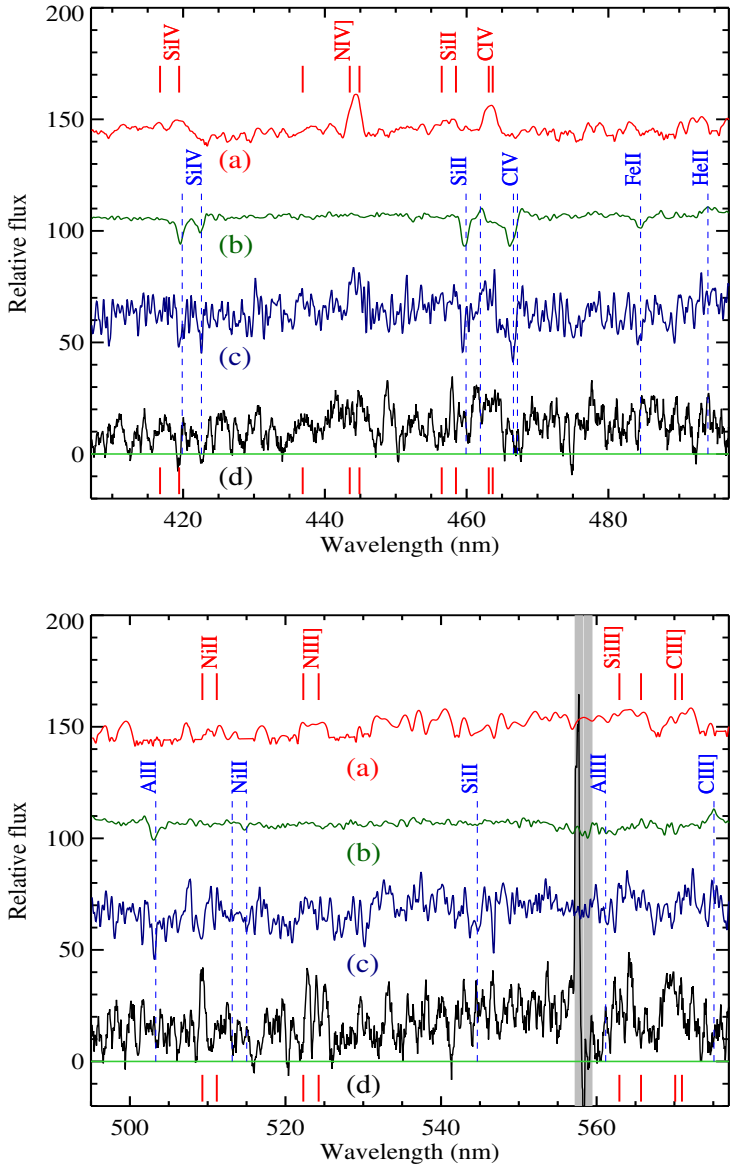

Figure 5: Four spectra with arbitrary vertical offsets to aid in SN 234161 emission-line identification. This plot is similar to Figure 2 in the main Letter but expanded into two wavelength sections for more detail. The four spectra are: (a) the low-redshift SN 1998S [13] (aged 485d) corrected to the redshift and observed velocity offset of SN 234161 ($z = 2.0125 - 2500$ km s^{-1}), (b) a $z \sim 3$ galaxy composite spectrum [30] corrected to $z = 2.0125$. (c) convolution of the SN 1998S and galaxy composite spectra with Gaussian noise added to match that of the data, and (d) the spectrum of SN 234161 (aged 365d). See text for details.